Published online 5 April 2022

Nucleic Acids Research, 2022, Vol. 50, No. 7 ***3693–3708***
https://doi.org/10.1093/nar/gkac217

Nonmodular oscillator and switch based on RNA decay drive regeneration of multimodal gene expression

Benjamin Nordick[1], Polly Y. Yu[2], Guangyuan Liao[3] and Tian Hong[3,4,*]

[1]School of Genome Science and Technology, The University of Tennessee, Knoxville, Tennessee 37916, USA, [2]NSF-Simons Center for Mathematical and Statistical Analysis of Biology, Harvard University, Cambridge, Massachusetts 02138, USA, [3]Department of Biochemistry & Cellular and Molecular Biology, The University of Tennessee, Knoxville, Tennessee 37916, USA and [4]National Institute for Mathematical and Biological Synthesis, Knoxville, Tennessee 37916, USA

Received January 05, 2022; Revised March 13, 2022; Editorial Decision March 19, 2022; Accepted March 21, 2022

ABSTRACT

Periodic gene expression dynamics are key to cell and organism physiology. Studies of oscillatory expression have focused on networks with intuitive regulatory negative feedback loops, leaving unknown whether other common biochemical reactions can produce oscillations. Oscillation and noise have been proposed to support mammalian progenitor cells' capacity to restore heterogenous, multimodal expression from extreme subpopulations, but underlying networks and specific roles of noise remained elusive. We use mass-action-based models to show that regulated RNA degradation involving as few as two RNA species—applicable to nearly half of human protein-coding genes—can generate sustained oscillations without explicit feedback. Diverging oscillation periods synergize with noise to robustly restore cell populations' bimodal expression on timescales of days. The global bifurcation organizing this divergence relies on an oscillator and bistable switch which cannot be decomposed into two structural modules. Our work reveals surprisingly rich dynamics of post-transcriptional reactions and a potentially widespread mechanism underlying development, tissue regeneration, and cancer cell heterogeneity.

GRAPHICAL ABSTRACT

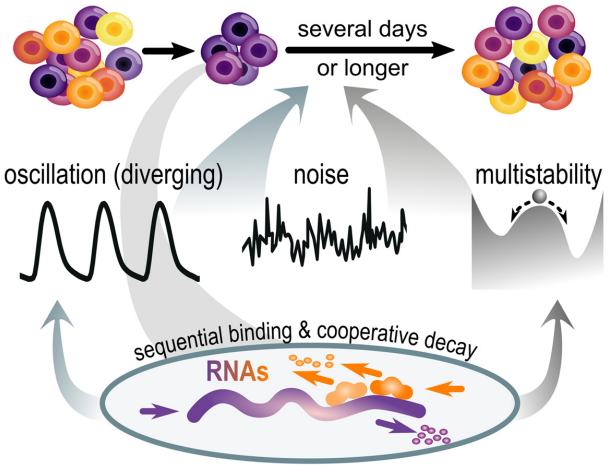

INTRODUCTION

Gene expression variations caused by non-genetic factors are widely observed in mammalian cells (1–5). These variations have functional consequences such as altered differentiation potentials of stem cells and drug resistance of cancer cells (1–3,6,7). For progenitor cells that exhibit multimodal expression patterns, a small subpopulation with a relatively homogenous expression profile recovers the parental population's heterogeneity of individual gene products after several days or longer (2,8–10) (Figure 1 box). Although stochasticity in transcriptional activities can cause expression variation and associated cell state changes (3,11), this type of noise influences expression at a much faster timescale (minutes) than the fluctuations required to achieve observed cell state transitions (days) (1,2,8,12,13). It was proposed that deterministically oscillatory dynamics may also be necessary for the recovery of

*To whom correspondence should be addressed. Tel: +1 865 974 3089; Email: hongtian@utk.edu

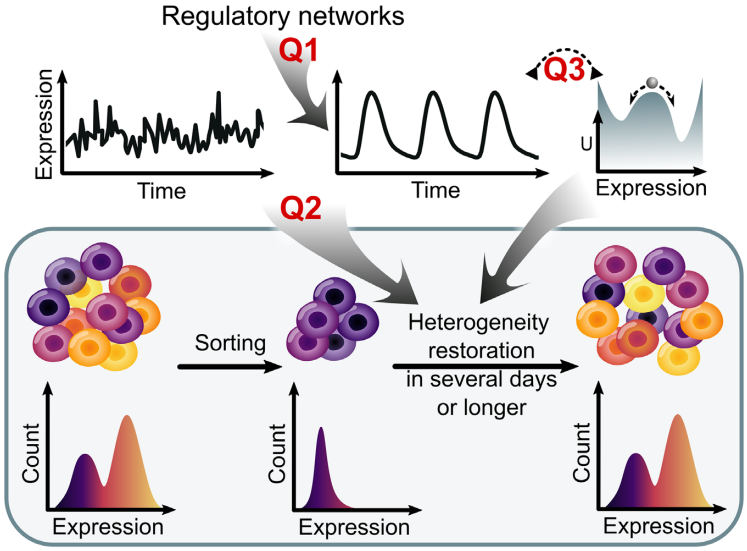

Figure 1. Questions related to dynamics of heterogeneity restoration process of expression patterns in progenitor or cancer cells. The study aims to provide insights into three questions: 1) Is there a widespread and hitherto unknown regulatory network structure that can generate oscillatory dynamics of gene expression at timescales of days? 2) How do oscillation and stochasticity work together to drive restoration of heterogeneity from a subpopulation with relatively homogeneous expression patterns? 3) How can the theories of multistability and oscillation be reconciled in the context of heterogeneity restoration and multimodal distribution of gene expression?

heterogeneity (9,14,15), but instances of transcriptional network structure (e.g. transcriptional negative feedback loop) supporting the observed dynamics have not been found experimentally. Furthermore, how stochasticity works together with oscillation to recover cellular heterogeneity remains elusive. Finally, the multimodality of the expression patterns suggests the possibility of multistability (i.e. coexisting point attractors, Figure 1 top right) (14,16). While both oscillatory and multistable systems allow slow cell state changes, they seem to contradict each other in terms of the underlying regulatory networks (17), and it is unclear which mechanism restores the heterogeneous patterns more robustly.

Most human mRNA transcripts are subject to microRNA-mediated regulation at the post-transcriptional level (18). Earlier findings indicated that microRNAs reduce gene expression noise through feed-forward loops (19). More recently, however, it was shown that microRNA can also increase the variability in gene expression via more basic molecular mechanisms such as triggering mRNA degradation (8,20,21). In particular, the loss of microRNAs led to significantly reduced expression heterogeneity in embryonic stem cells (8), and the lack of a microRNA binding site on a target mRNA dampened the oscillation of the target's expression in neural progenitor cells (22). These observations suggest versatile dynamics of microRNA-mRNA reaction networks and potential functions in maintaining heterogeneity in progenitor cells. Recent theories postulated that these reaction networks can produce positive-feedback-like dynamics such as bistability (23,24), but it remains unclear whether more diverse types of dynamical features, such as oscillations, can be generated by the RNA-centric interactions.

Based on recent data of mRNA-microRNA interactions through multiple microRNA binding sites, we used mass-action kinetics to build mathematical models for simple post-transcriptional reaction networks. These networks potentially describe the dynamics of transcripts from nearly half of human protein coding genes. Through computational analysis of these common reaction networks, we identified regions of biologically plausible kinetic rate constants that give rise to sustained oscillations, despite the apparent absence of any explicit feedback loop typically considered necessary for oscillation. We found that the regions corresponding to oscillation and bistability overlap, which not only confers dual functions to the systems, but also allows excitability and abruptly diverging period of oscillations. The emergent dynamics provide a new explanation for the experimentally observed heterogeneity and multimodality regeneration effects of microRNAs on timescales of days (8,20). Remarkably, we found that oscillation and bistability require the same simple set of molecular species, which revealed a dual-function network without structural modularity. Our results uncover surprisingly rich dynamics of post-transcriptional reaction networks widespread in biology and a previously underappreciated mechanism for regenerating multimodal gene expression in cell populations.

MATERIALS AND METHODS

Model construction

All mRNA-microRNA models in this study are based on mass-action kinetics. The first model considers an mRNA with one microRNA binding site (the MMI1 Model), and the other models consider an mRNA with two microRNA binding sites (the MMI2 Models). The ordinary differential equation (ODE) models were nondimensionalized by scaling the variables and parameters with the degradation rate constant of the mRNA and the synthesis rate constant

of the microRNA. One time unit corresponds to approximately $1.44 \times t_{1/2}$ where $t_{1/2}$ is the half-life of the mRNA. For visualizing dynamical systems underlying the models, we applied the total quasi-steady state assumption (tQSSA) (25–27) and reduced each model to two ODEs. The full models were used in all simulations and bifurcation analyses. The 2-dimensional models were used to construct phase planes and the determinant-trace plots for their Jacobian matrices. The two versions of the model gave consistent results.

Parameter sampling and numerical bifurcation analysis

To investigate the possible dynamical features of the models, 10^5 parameter values were randomly selected for each model. The distributions of the parameters were estimated with known ranges of biologically plausible values (see Supplementary Data Section 1.5 and Supplementary Table S1). Synthesis rate constant of mRNA σ_R was used as the control parameter for numerical bifurcation analysis, which quantified the steady state signal-response relationship in the range $0 < \sigma_R < 25$. Local bifurcation points were detected using Tellurium (28). Limit cycles were followed using PyDSTool (29), which further provided the information for global bifurcations. Spiral sinks were detected by identifying complex eigenvalues of Jacobian matrix at the scanned stable steady states numerically.

Algebraic analysis

Using the Chemical Reaction Network Toolbox and its underlying theory (30), we determined the possibility of obtaining one or more positive steady state for each model. The stability of the steady state in models that admit only one positive steady state with any positive rate constants was determined by the Routh-Hurwitz Stability Criterion (31,32).

Estimation of occurrences of mRNA-microRNA models

Predicted microRNA-mRNA binding sites from TargetScan were used to determine possible occurrences of structures in which one mRNA molecule binds one or two microRNA molecules (33). Protein-coding genes that have one microRNA binding site were used to estimate the occurrence of the structure of the MMI1 Model: 2554 genes. For the MMI2 Models, we used protein coding genes that have more than one microRNA binding site: 10483 genes. We further used miRTarBase to obtain the number of genes, 12616, that can be targeted by two distinct microRNA families with experimental evidence supporting the microRNA-RNA binding (34). Among them, 8420 genes contain more than one microRNA binding site predicted by TargetScan. Although TargetScan may have many false positives, it is known that false negatives also exist. For example, TargetScan does not include the experimentally validated targeting of *Nanog* by miR-296 at two binding sites (35).

Estimation of occurrences of transcriptional negative feedback loops

Negative transcriptional feedback loops were enumerated using HiLoop (36) on the full network derived from the TRRUST version 2 database (37). Limiting loops to at most 3 genes for comparable complexity with the MMI Models, 52 negative feedback loops were found. Of the 2862 genes in the network, 62 were involved in at least one such negative feedback loop.

Stochastic simulation and quasi-potential landscape

We performed stochastic simulations for the MMI2 Model with two binding sites for the same microRNA using either additive or multiplicative noise in the ODEs. To select a cell state with a representative extreme expression pattern, we first solved the ODEs deterministically with 400 initial conditions and selected the state with either the lowest or the highest level of R_T in the period $40 < t < 200$. For one simulation of a cell population, we used this state as the initial conditions for 500 cells, and we solved the stochastic ODEs for another 200 time-units (38). Noise levels and other parameters were changed to examine the robustness of the bimodality regeneration. The simulation results were subsequently used to construct quasi-potential landscapes with potential $U(x) = -\log P_S(x)$, where $P_S(x)$ is the probability density function at the stationary phase ($t > 100$) (39). To consider intrinsic noise alone in an accurate manner, we implemented an additional form of stochastic simulation based on the Gillespie algorithm and propensity functions derived from mass-action kinetics. Using simulations of 200 cells, we examined the consistency between the stochastic ODEs and the Gillespie algorithm under different levels of noise and signals σ_R. The stochastic model with additive noise was also extended to capture the dynamics of cell proliferation (Section 2.1.10 in Supplementary Data).

Note that the Gillespie algorithm is accurate for mass-action kinetics describing elementary reactions, but not more phenomenological descriptions of reactions (40,41). All models in this study are based on mass-action kinetics, except for a repressilator model used for comparison (42). For the repressilator model, we only used stochastic ODEs for simulation. We used a mass-action-based negative feedback model (43) for additional comparison between our models and previously known oscillators. For accurate and straightforward implementation, we used the full Gillespie algorithm, rather than tQSSA-based approaches, which involve more sophisticated approximation (44). This is consistent with ODE simulations and bifurcation analysis which primarily consider the full mass-action systems.

Statistical analysis

Bimodality of cell populations was tested by comparing the Bayesian Information Criterion of a one-Gaussian fit of mRNA levels to a two-Gaussian fit. The two-Gaussian mixture models were further tested for distinguishability of the modes (45), requiring $|\mu_1 - \mu_2|/\sqrt{(\sigma_1^2 + \sigma_2^2)/2} > 2$.

RESULTS

An mRNA with one microRNA binding site generates spiral sinks but not oscillation or bistability

We used mass action kinetics to describe the dynamics of an mRNA and a microRNA with ordinary differential

equations (ODEs). In the first model, we considered an mRNA with one binding site for the microRNA (the MMI1 Model, Figure 2A). The two molecular species can bind to each other and form a complex. Each species is produced through transcription and is degraded both in its unbound form and in the complex. We simplified the mass-action-based model (see Supplementary Data Section 1) into the dimensionless form

$$\begin{aligned} dR/dt &= \sigma_R - \kappa^{\text{on}} Rr + \kappa^{\text{off}} C - R + \beta\gamma C \\ dr/dt &= 1 - \kappa^{\text{on}} Rr + \kappa^{\text{off}} C - \gamma r + \alpha C \\ dC/dt &= \kappa^{\text{on}} Rr - \kappa^{\text{off}} C - \alpha C - \beta\gamma C. \end{aligned} \quad (1)$$

In this model, the three variables R, r and C represent the dimensionless (scaled) concentrations of unbound mRNA, unbound microRNA, and mRNA-microRNA complex respectively. The parameters (Greek letters) were also scaled, and each is related to a biologically meaningful parameter. σ_R represents the transcription rate constant of mRNA and can be considered a signal input. κ^{on} represents the association rate constant. κ^{off} represents the dissociation rate constant. The scaled dissociation constant $\mathrm{K} = \kappa^{\text{off}}/\kappa^{\text{on}}$. The degradation rate constant of unbound mRNA and the microRNA production rate constant were scaled to 1 (see more details in Supplementary Data Section 1.1). The degradation rate constant of unbound microRNA is represented by γ. We define α and β as regulated degradation factors (RDFs). α represents how fast mRNA is degraded in the complex relative to its unbound form, and β is the corresponding factor for microRNA. These two RDFs are important because the gene regulatory function of microRNA primarily depends on the target mRNA degradation upon binding (46), and similarly, the target mRNA can alter the degradation rate constant of the mRNA-bound miRNA (47). Here, we assumed that mRNA and microRNA are degraded independently in the complex, which is supported by previous observations (47–49). Equation 1 can be simplified with representation of rapid chemical processes (e.g. binding and unbinding) using algebraic equations and change of variables to R_{T} and r_{T}, which represent the total scaled concentrations of the mRNA and the microRNA respectively (26,27) (see Supplementary Data Section 1.2).

To explore the possible dynamical behaviors of the MMI1 Model, we randomly generated 10^5 parameter sets with biologically plausible values. Each parameter value was chosen from a range covering at least two orders of magnitude (see Section 1.5 in Supplementary Data for estimation of each parameter). Through numerical bifurcation analysis with respect to signal σ_R, which shows steady state signal-response relationships, we found that each parameter set gave rise to a single stable steady state, i.e. point attractor (Figure 2B shows two representative signal-response curves). Nonetheless, we found that 13.4% of parameter sets generated extremely transient oscillations in narrow ranges of σ_R (Figure 2B-C, Supplementary Figures S2 through S4). In the deterministic systems studied here, we define *sustained oscillation*, abbreviated *oscillation*, as limit cycle oscillation, which is a long-term periodic dynamical pattern. In contrast, *damped oscillation* is transient, characterized by a spiral trajectory which eventually converges to a point attractor, i.e. a spiral sink (Figure 2C) (50). Regardless of whether the damped oscillation was present, the response curves with respect to σ_R show that with a single binding site, the microRNA enabled a threshold at which the unbound mRNA concentration starts to increase significantly (Figure 2B, Supplementary Figure S3), consistent with previous experimental data and models (51). Furthermore, the presence of the microRNA only gave rise to moderate (< 10-fold) changes of the total mRNA concentrations (Supplementary Figure S3). This is consistent with the commonly observed moderate effects of microRNA on protein production, showing that the selected values of RDFs and other parameters in our models are realistic. Interestingly, the damped oscillations primarily occurred near the thresholds (estimated as the level of σ_R at $R = 0.1$, denoted by $\hat{\sigma}_R$) of the unbound mRNA activation (Supplementary Figure S3A) and required negatively correlated RDFs (Figure 2D). In general, the damped oscillations did not strongly depend on the choice of specific values for individual parameters (Supplementary Figure S4).

We next used algebraic approaches to corroborate the computational results. We found that the MMI1 Model gives rise to a single stable steady state with any arbitrary combination of positive rate constants (Sections 1.3 and 1.4 in Supplementary Data, Supplementary Figure S1), suggesting that some additional structural component (i.e. molecular species) is required to achieve oscillation.

Multiple microRNA binding sites enable sustained oscillation and bistability without explicit feedback

In this section, we discuss several variants of the MMI2 Model that describes an mRNA with two binding sites for one or two microRNAs, a biological system more common (see Methods) than the one captured by the MMI1 Model. The inclusion of additional binding sites permits several possibilities in terms of the binding reactions, but we first considered a very basic mechanism of binding: one microRNA binds to the two sites independently with equal affinities. This assumption gave rise to two 1:1 complexes, each with a microRNA molecule bound to the first site (Site 1) or the second site (Site 2) on the mRNA, respectively (Figure 3A). Because these two complexes were assumed to have identical kinetic properties, their concentrations are always equal in a deterministic system. We therefore used a single state variable C_1 to describe the concentration of each complex. Under this assumption, a 2:1 complex, with concentration denoted by C_2, is formed when the microRNA binds to either 1:1 complex. We named this version of the MMI2 Model with symmetrically sequential binding the MMI2-SSB Model, which is given by

$$\begin{aligned} dR/dt &= \sigma_R - 2\kappa^{\text{on}} Rr + 2\kappa^{\text{off}} C_1 - R + 2\beta_1\gamma C_1 \\ dr/dt &= 1 - 2\kappa^{\text{on}} Rr + 2\kappa^{\text{off}} C_1 - 2\kappa^{\text{on}} C_1 r \\ &\quad + 2\kappa^{\text{off}} C_2 - \gamma r + 2\alpha_1 C_1 + 2\alpha_2 C_2 \\ dC_1/dt &= \kappa^{\text{on}} Rr - \kappa^{\text{off}} C_1 - \kappa^{\text{on}} C_1 r + \kappa^{\text{off}} C_2 - \alpha_1 C_1 \\ &\quad - \beta_1\gamma C_1 + \beta_2\gamma C_2 \\ dC_2/dt &= 2\kappa^{\text{on}} C_1 r - 2\kappa^{\text{off}} C_2 - \alpha_2 C_2 - 2\beta_2\gamma C_2. \end{aligned} \quad (2)$$

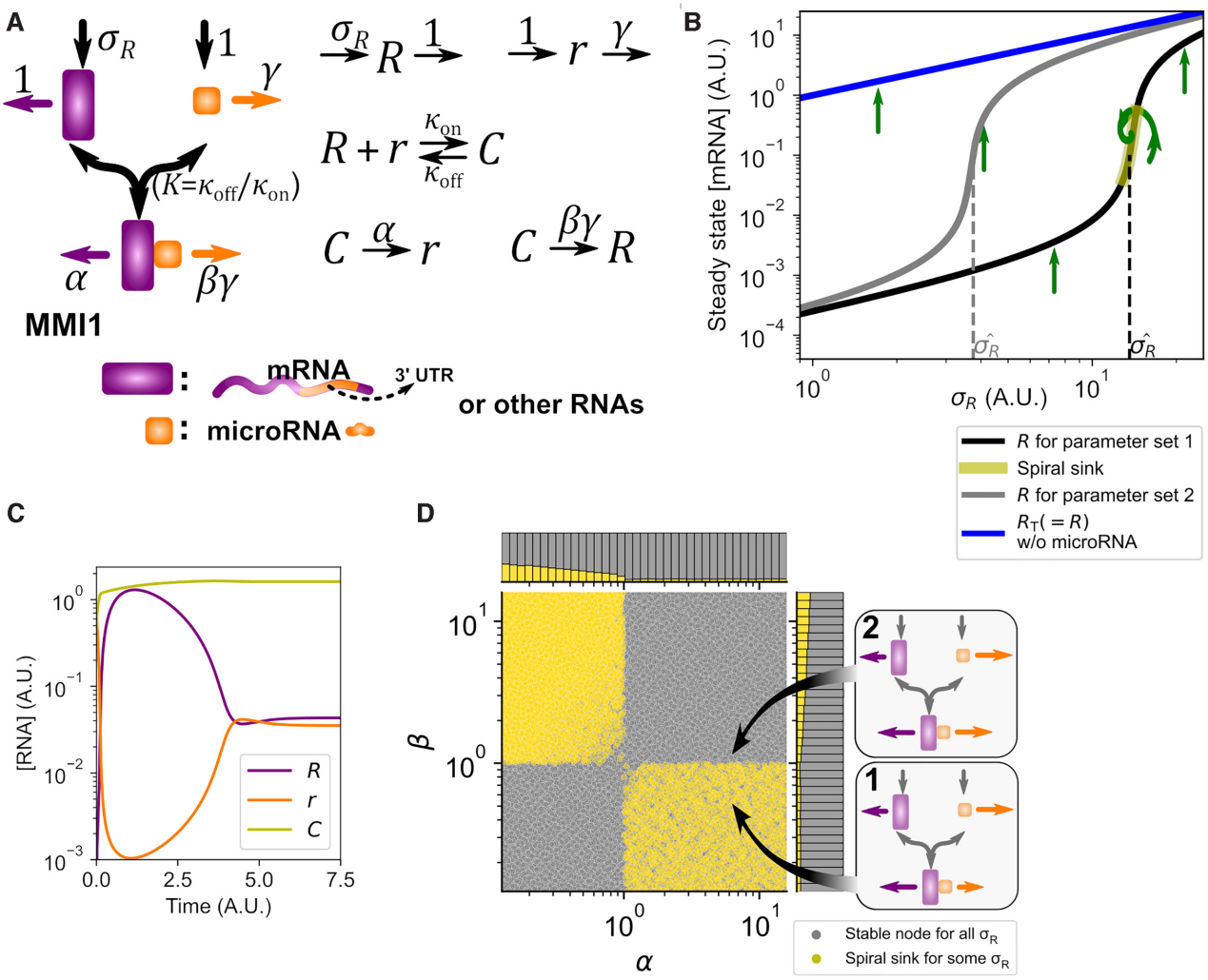

Figure 2. Dynamics of the MMI1 Model. (**A**) Left: illustration of reaction network of the MMI1 Model. Purple icon represents mRNA. Orange icon represents microRNA. Horizontal arrows represent degradation. Straight vertical arrows represent synthesis. Curved arrows represent binding. Right: eight chemical reactions associated with the MMI1 Model, which describes the dynamics of each molecular species with the law of mass-action (equation 1 and Supplementary Data Section 1). UTR, untranslated region. (**B**) Two representative signal-response curves (black and gray) showing steady state levels of R in response to transcription rate constant σ_R. Green arrows indicate the type of these steady states: straight arrows show stable nodes and spiral arrow shows spiral sinks. Blue curve shows the microRNA-free response for both parameter sets. (**C**) Time-course simulation showing transient oscillation near a spiral sink (parameter set 1). One time unit is approximately $1.44 \times t_{1/2}$ where $t_{1/2}$ is the half-life of the mRNA. (**D**) Distribution of the parameter sets with spiral sink steady state (yellow, e.g. parameter set 1) and those without (gray, e.g. parameter set 2) in the space of two representative parameters (RDFs). Callouts illustrate the two representative parameter sets (same as those in B) with degradation rate constants represented by arrow lengths. Only the values of β differ between the two sets. Marginal distributions are shown in stacked bars.

Similar to the MMI1 Model, this model can be reduced to two dimensions representing 'slow' variables R_T and r_T (see Supplementary Data Section 2.1.3). Strikingly, when we used the sampling strategy described earlier, we found many biologically plausible parameter sets that produced sustained oscillations at some σ_R (9.4% of the 10^5 sets; Figure 3B-C, Supplementary Figures S5-S7). In this scenario, the system undergoes a Hopf bifurcation that leads to limit cycle oscillations at intermediate levels of σ_R (Figure 3B blue shade and top right phase plane). Further increase of σ_R gives rise to another Hopf bifurcation point which marks the approximate upper bound in the σ_R axis for limit cycle oscillations. In the example shown in Figure 3B, the Hopf bifurcation point at higher σ_R is subcritical, producing both an unstable limit cycle (dashed blue curve) and a stable limit cycle (solid blue curve) that appears abruptly.

With representative parameter sets, damped oscillations occurred at high levels of σ_R (Figure 3B yellow shade and lower right phase plane). Unlike the extremely transient oscillations with the MMI1 Model, these damped oscillations can have significantly long durations (Figure 3C) and can be observed in wide ranges of parameter values including σ_R (Figure 3E, Supplementary Figure S5). In the limit cycle oscillations, dramatic variations in fold change of unbound mRNA and microRNA were observed (Figure 3B, C purple and orange), whereas moderate (≈3-fold) changes of total mRNA occurred, again confirming the moderate

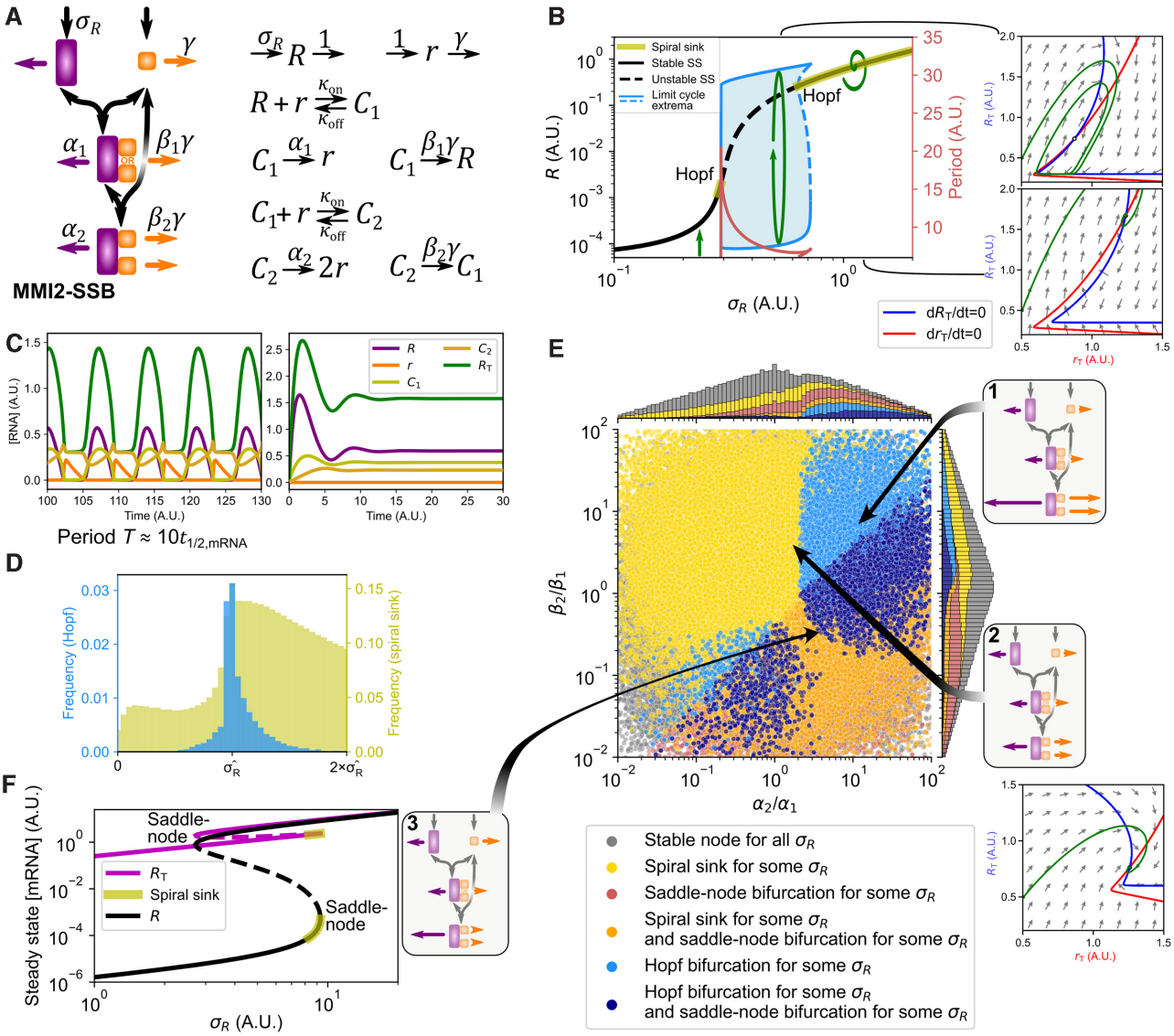

Figure 3. Dynamics of the MMI2-SSB Model. (**A**) Left: illustration of reaction network of the MMI2-SSB Model. Purple icon represents mRNA. Orange icon represents microRNA. Right: twelve chemical reactions associated with the MMI2-SSB Model in equation 2, which describes the dynamics of each molecular species with the law of mass-action. (**B**) Left: bifurcation diagram showing levels of R in response to transcription rate constant σ_R. Green arrows illustrate the type of these steady states: straight arrow shows stable node, spiral arrow shows spiral sinks, and circulating arrow shows limit cycles. Blue shade: limit cycles' inner basins of attraction. Right: phase planes (constructed with the 2D version of the MMI2-SSB Model) show sustained ($\sigma_R = 0.5$, top) and transient oscillations ($\sigma_R = 1$, bottom). Open circle represents unstable steady state. Blue and red curves are nullclines. Green curves show representative solutions. Other parameter values: $K = 0.001, \gamma = 0.25, \alpha_1 = \beta_1 = 1, \alpha_2 = 12, \beta_2 = 7$. A basal synthesis rate constant $\sigma_R^0 = 3.1$ was added to the ODE for R. (**C**) Time-course trajectories for the two scenarios shown in B. One time unit is approximately $1.44 \times t_{1/2}$ where $t_{1/2}$ is the half-life of the mRNA. (**D**) Yellow histogram shows the distribution of the spiral sink steady states relative to the position of the threshold transcription rate constant $\hat{\sigma}_R$ at which $R = 0.1$. Blue histogram shows the distribution of Hopf bifurcation points. (**E**) Left: distribution of the parameter sets with various types of steady states obtained with bifurcation analysis with respect to σ_R in the space of the RDF ratios. Callouts show representative parameter sets with arrow lengths representing degradation rate constants (Set 1 was used for results shown in B and C). Phase plane shows a transient oscillation obtained with Set 2. Marginal distributions are shown in stacked bars. (**F**) Left: bifurcation diagram showing the steady states of unbound mRNA and total mRNA with respect to σ_R. Solid curves: stable steady states. Dashed curves: unstable steady states. Right: illustration of Set 3 whose behavior is shown. Parameter values: $K = 0.001, \gamma = 2, \alpha_1 = 1, \beta_1 = 0.5, \alpha_2 = 4, \beta_2 = 0.1$.

overall effect of microRNA (blue curves in Figure 3B phase planes and Figure 3C). With the parameter set that enabled sustained oscillation, we found that the period of the oscillation was approximately 10 times of the half-life of the mRNA (Figure 3C), which corresponds to at least one day for typical mammalian mRNAs (52). Nonetheless, a wide range of periods for biological rhythms might be obtained by the model given the wide distribution of mRNA half-lives (52). More importantly, the period increased steeply when the signal approached the Hopf bifurcation near the activation threshold (Figure 3B red). We will examine the significance and the source of this phenomenon in a later section.

With an estimated threshold of 0.1 units of unbound mRNA, we found that many Hopf bifurcation points were located near the activation threshold, whereas the damped oscillations primarily appeared in the high σ_R region (Figure 3D). The Hopf bifurcation points were distributed very widely in the space of all other parameters (Supplementary Figure S6). To illustrate the regions corresponding to these bifurcations, we focused on a phase space of RDF ratios for the two RNAs, i.e. α_2/α_1 and β_2/β_1 (Figure 3E). These ratios represent how fast the mRNA and the microRNA are degraded in the 2:1 complex relative to their degradation rate constants in the 1:1 complex, and can be viewed as a functional cooperativity, or synergy, between the two microRNA binding sites. We use the term *functional cooperativity* here to distinguish it from binding cooperativity that often describes the enhanced or reduced binding affinity of a second site upon the binding to the first site. Previous observations suggested that in most cases the two sites have a positive functional cooperativity in terms of the degradation rate constants of mRNAs, and in fact the $\alpha_2 : \alpha_1$ ratios are often equal to or greater than 2 (53). The RDF ratio for microRNA (β_2/β_1) has not been systematically characterized, but we permitted both positive and negative cooperativities. Very interestingly, most Hopf bifurcations and their associated oscillations appeared in a region where RDF ratios (α_2/α_1 and β_2/β_1) are both high (e.g. Parameter Set 1 in Figure 3E), whereas a small fraction of Hopf bifurcations were observed with low RDF ratios (Figure 3E lower left region). Damped oscillations were observed in 41.8% of parameter sets (Figure 3E yellow and orange), including areas of RDF ratio space where Hopf bifurcations were absent (e.g. Parameter Set 2 and phase plane in Figure 3E).

In addition to oscillations, we found that a large number of parameter values (31.7%) generated bistable systems characteristic of biological switches (e.g. Parameter Set 3 in Figure 3E-F), a conclusion consistent with previous studies (23,24). Like oscillations, the bistable switches involved dramatic changes of unbound mRNA concentration and moderate changes of total mRNA concentrations (Figure 3F). Bistable switches with respect to signal σ_R were observed only if the inequality

$$\alpha_2/\alpha_1 > 2\beta_2/\beta_1 \quad (3)$$

was satisfied (Figure 3E, boundary between light blue and dark blue regions).

We found that the two parameter regions corresponding to oscillation and bistability respectively had a significant overlap in the space of RDF ratios (Figure 3E, dark blue), and we will explore this result in a later section. In addition to the RDF ratios, we found that the existence of the sustained oscillations depends on the choice of γ. In our simulations, the median of the distribution for γ was chosen to be 0.25, which is supported by previous experimental studies (54). We observed that the oscillations were obtained with high RDF ratios (high α_2/α_1 and high β_2/β_1) when γ was low, whereas oscillations with low RDF ratios required high γ (Supplementary Figure S7). Nonetheless, many biologically plausible values of the parameters in the MMI2-SSB Model, including the median values of distributions for γ and K in our sampling experiments, gave rise to bistability and oscillation (Supplementary Figure S7). In addition, we found that coregulated transcription of microRNA and its target significantly expanded the parameter region for limit cycles (Supplementary Figure S8). This type of coregulation may be achieved by localization of a microRNA gene in the intronic region of its target gene, e.g. *mir-196* and its target *Hoxb7* (55).

The dynamical profile shown in Figure 3B provides a possible explanation for recent data that showed perplexing roles of microRNAs: Schmiedel et al. and Wei et al. found that microRNA reduces variability of gene expression for lowly expressed genes but increases the variability for highly expressed genes (20,21). While the increased variability could be explained by additional stochasticity introduced by microRNA-mediated regulations (20), our analysis suggests that the observed variability of highly expressed genes controlled by microRNAs could alternatively be due to the spiral nature of the steady state, which may also be related to functional rhythms. Nonetheless, the observation of limit cycle oscillations in the MMI2-SSB Model is surprising because the network structure does not contain any explicit negative feedback loop, a structure considered a necessary condition for biological oscillators (56). While it is remarkable that a simple system containing so few molecular species can possess very diverse dynamical features (e.g. oscillation and bistability), which can arise even without apparent appearance of feedback loops, we inferred implicit feedback in the MMI2-SSB Model from representative numerical values of rate constants (Supplementary Figure S9).

We next asked whether the observed oscillation and bistability were sensitive to the assumption that the two binding sites were identical in terms of kinetic properties, or the fact that the two 1:1 complexes were described by a single variable C_1 in the model. We therefore considered a modified MMI2 Model in which the binding of microRNA to Site 2 on mRNA requires the binding of Site 1. This asymmetrically sequential binding model, named MMI2-ASB Model, now contains a unique 1:1 complex corresponding to the first binding site occupied by the microRNA (Figure 4A). We found that this model generated results similar to the MMI2-SSB Model in terms of the parameter regions for oscillation and bistability: 8.4% of parameter sets gave rise to Hopf bifurcation and oscillations, whereas 29.6% of parameter sets produced bistable switches (Figure 4B, Supplementary Figure S16). Because the two binding sites in the MMI2-ASB Model were assumed to be distinct, we asked whether the difference in the binding affinity (described by the dissociation constant K) can influence the emergence of oscillation and bistability. To test this, we randomly chose K_1 (the scaled dissociation constant for Site 1) as before and set K_2 (for Site 2) equal to K_1 multiplied by a constant. We found that positive binding cooperativities ($K_2 < K_1$) had a negative effect on producing oscillation and bistability, whereas negative binding cooperativities ($K_2 > K_1$) (57) enhanced the ability to generate oscillation and bistability until the binding affinity for Site 2 became too low (Figure 4C). Nevertheless, large numbers of parameter sets produced spiral sinks, oscillation and bistability over a wide range of $K_2 : K_1$ ratios.

Because cooperativity among multiple microRNAs in cellular functions has been observed previously (58–60), we asked whether the conclusions about oscillation and bista-

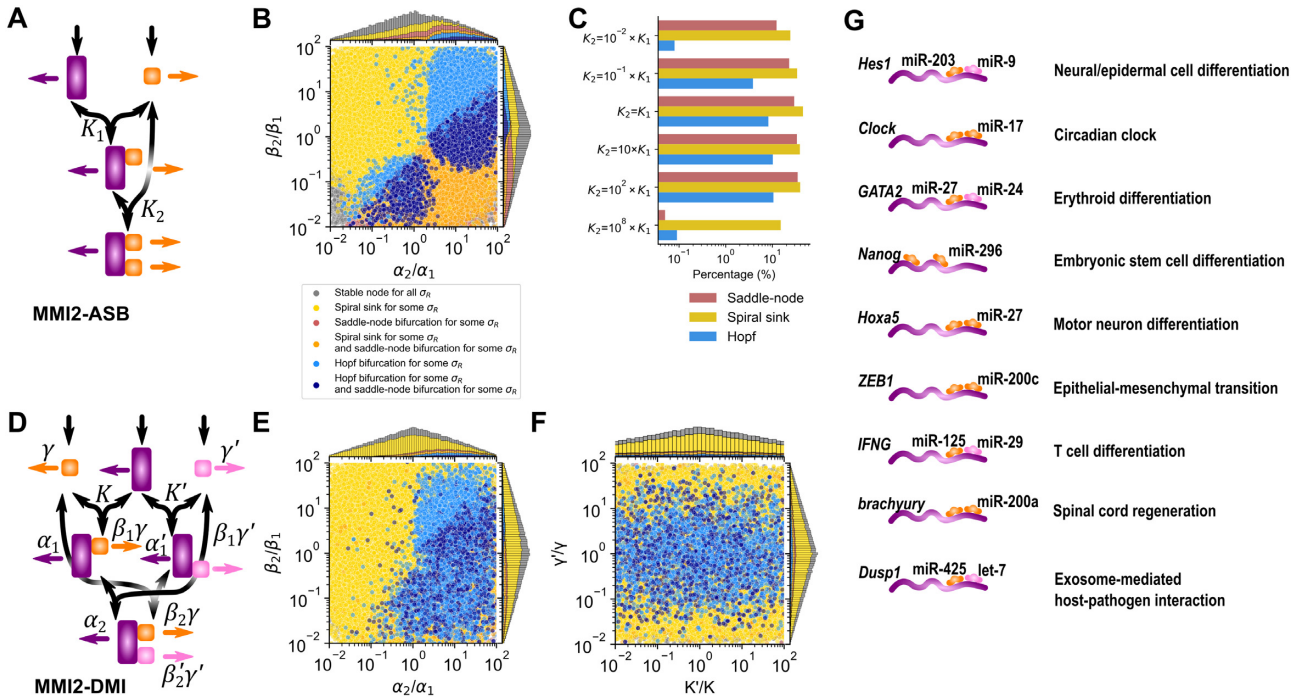

Figure 4. Dynamics of the MMI2-ASB and MMI2-DMI Models. (**A**) Illustration of the MMI2-ASB reaction network. (**B**) Distribution of the randomly selected parameter sets for MMI2-ASB with various types of steady states obtained with bifurcation analysis with respect to σ_R in the space of the RDF ratios. (**C**) Percentages of parameter sets with various types of steady states obtained with bifurcation analysis with respect to σ_R. Parameters were randomly selected as in B, except for K_2 which was equal to K_1 multiplied by the indicated factors. (**D**) Illustration of the MMI2-DMI reaction network. Orange and pink icons represent two different microRNAs. (**E**) Distribution of the randomly selected parameter sets for MMI2-DMI with various types of steady states obtained with bifurcation analysis with respect to σ_R in the space of the RDF ratios. Parameter values for the two microRNAs are uncorrelated. (**F**) Same data as in E shown in the space of ratios between the parameters for the two microRNAs. In B, E and F, marginal distributions are shown in stacked bars. (**G**) Examples of MMI2 systems with experimental evidence that support direct binding. These circuits are relevant to neural or epidermal cell differentiation (61,62), circadian rhythm (63), erythroid differentiation (64), embryonic cell differentiation (35), motor neuron differentiation (23,65), epithelial-mesenchymal transition (66), T cell differentiation (67,68), spinal cord regeneration (69), and host-pathogen interaction (59) respectively.

bility with the MMI2 Models can be extended to the scenario where the two binding sites are recognized by two different microRNAs. In this dual-microRNA model (the MMI2-DMI Model, Figure 4D), two microRNAs were explicitly described and assumed to each bind only their respective site. As expected, with the assumption that the two microRNAs have identical rate constants, the MMI2-DMI Model had similar performance as the MMI2-SSB Model: 8.7% of parameter sets produced oscillation, and 28.8% of parameter sets produced bistability. With the assumption that the two binding sites have distinct, independently chosen dissociation constants and other associated parameters such as RDFs, we again observed similar results in terms of the capacity of oscillation (4.9%) and bistability (13.8%). These dynamical features did not require high similarities of the two microRNAs or the two binding sites (Figure 4E-F).

We have shown that under several different assumptions, the MMI2 Models generated spiral sinks, oscillation and bistability in biologically plausible parameter regions. We asked how many human protein-coding genes may be directly involved in the MMI Models. With TargetScan, a microRNA binding site prediction program, we found 2554 human protein-coding genes whose 3' untranslated regions contain only one conserved microRNA binding site (the structure of the MMI1 Model), whereas 10483 genes were predicted to contain two or more conserved binding sites (the structures of the MMI2 Models) (33). Furthermore, according to miRTarBase (34), for 8420 of the genes with two putative binding sites, there is experimental evidence that supports two or more microRNA families both targeting each gene, as in the MMI2-DMI Model structure. We therefore estimate that nearly half of human protein-coding genes are involved in the structures of the MMI2 Models. In contrast, only 62 genes were predicted to be involved in transcriptional negative feedback loops with up to three edges (see Methods). Several examples of the MMI2-like systems with experimental evidence of RNA binding and functional significance are shown in Figure 4G (23,35,59,61–69). While the kinetic rate constants of these systems have not been measured systematically, it was observed that multiple microRNA binding sites can have additive and ultra-additive cooperativities in terms of mRNA degradation ($\alpha_2/\alpha_1 \geq 2$) (53,58,70). The oscillatory dynamics emerged from the MMI2 Models were flexible in terms of the type of multi-site cooperativity for microRNA degradation (β_2/β_1 can be equal to, greater than, or less than 1) (Figures 3B and 4B, right blue regions).

In the next sections, we first discuss the characteristic global features of MMI2-driven dynamics beyond saddle-node and Hopf bifurcations. Next, we explore the possible biological functions of the microRNA-driven oscillators.

Finally, we test the decomposability of the MMI2 Model into an oscillator module and a bistable switch module with distinct molecular compositions.

Multiple microRNA binding sites enable global bifurcation and robust regeneration of heterogenous expression

Because the Hopf bifurcations and bistable switches both occurred near the thresholds of the mRNA activation (Figure 3D), we hypothesized that the MMI2-SSB Model can generate global bifurcations with features not captured by the local Hopf and saddle-node bifurcations. We examined the parameter sets that gave rise to both Hopf and saddle-node bifurcations with respect to σ_R (Figure 3E dark blue) and found that all of them produced global bifurcations: about one third of the sets generated saddle-node on invariant circle (SNIC) bifurcations and the rest generated saddle-loop bifurcations (Figure 5A). During SNIC bifurcation, a saddle-node bifurcation point collides with a limit cycle (Figure 5B), giving rise to an abrupt appearance of periodic trajectories as σ_R increases gradually (e.g. Figure 5C-D). The limit cycle eventually disappears through a Hopf bifurcation with further increase of σ_R. The periods of limit cycles diverge dramatically near the SNIC bifurcation point, going to infinity at the bifurcation point (Figure 5B, red).

Oscillators that appear abruptly with diverging periods give rise to a particular type of excitability that is known to govern asynchronous oscillators, Class I excitability (Figure 5B red bar) (71). We therefore hypothesized that the period-diverging property can be used to generate heterogeneous gene expression pattern in the presence of noise that may result from stochasticity in transcription. We first simulated the MMI2-SSB Model with additive transcriptional noise in RNA production and a σ_R level close to the SNIC bifurcation point. With an identical initial condition for multiple simulated cells, we observed asynchronous fluctuations of mRNA levels (Figure 5E). The fluctuations contained both moderate, frequent changes, and dramatic, infrequent changes of mRNA levels. We define the latter as cell state changes. With 500 simulated cells starting from a low mRNA condition, significant cell state changes at the population level occurred only after at least one mRNA half-life (Figure 5F). The gene expression pattern of the simulated cell population exhibited a damped oscillation and eventually converged to a bimodal distribution with stabilized fractions. The recovery of bimodal distribution from a selected homogeneous population, the slow onset of cell state transitions, and the nonmonotonic changes of gene expression distribution were consistent with previous observations in haematopoietic progenitor cells (2). Furthermore, the role of microRNA in multimodality regeneration at the timescale of days is consistent with recent observations in embryonic stem cells (8). Our results suggest that the mechanisms underlying these features may include diverging oscillations with the influence of both SNIC-like dynamics and stochasticity.

Although SNIC bifurcation was observed in a relatively small number of parameter sets, its key features extend to a wide region. Sudden oscillation appearance and rapid period change also occurred in scenarios without a SNIC bifurcation. For a saddle-loop bifurcation, an unstable limit cycle is first generated by a Hopf bifurcation as σ_R increases (Figure 5G-J). When σ_R increases further, a saddle point collides with the limit cycle, resulting in an abrupt disappearance of the limit cycle. Even for an oscillation-enabling parameter set without any global bifurcation, a limit cycle's period, though finite, changes sharply near a Hopf bifurcation point (Figure 3B). Because the SNIC bifurcation organizes a parameter region that generates limit cycles with rapid changes in period, we named the mechanism in the nearby parameter region a *diverging oscillator*.

Reversible cell state transitions and bimodal distribution of expression may alternatively be explained by a model describing two stable steady states (e.g. two point attractors, Figure 3F). This *bistable switch* mechanism has been very widely used to explain cell states and their transitions (72–76). We found that both diverging oscillator and bistable switch mechanisms produced bimodal distributions of gene expression at a basal level of transcriptional noise. To visualize the two distinct dynamical systems under both deterministic and stochastic influences, we plotted the quasi-potential landscapes for both mechanisms based on the results of stochastic simulations (Figure 6A-D). Consistent with the bimodal gene expression distributions, both mechanisms generated double-well potentials along the total mRNA axis. However, we observed a striking difference between the two mechanisms in their routes for state transitions: because of the limit cycle, the diverging oscillator has two "channels" connecting the two potential wells (Figure 6A cyan), whereas the two wells in the bistable switch mechanism are separated by a saddle point and its associated separatrix (Figure 6B yellow and orange). The double-channel-double-well landscape of the diverging oscillator allows rapid transition between two states driven by deterministic vector field, while the double-well landscape of the bistable switch only allows stochastic transitions between the two states (see blue representative trajectories in Figure 6A-B and Supplementary Video S1). Because of this difference, we hypothesized that the gene expression pattern driven by the bistable switch is more sensitive to the initial conditions and the noise levels. We therefore compared the performance of the two mechanisms in terms of bimodality regeneration with three levels of noise, two initial conditions, and three signal strengths. We first focused on the selected signal strengths σ_R allowing both mechanisms to produce bimodal distributions of mRNA expression at $t = 100$ (equivalent to 576 hours after cell sorting, assuming a 4-hour mRNA half-life) with the same levels of noise and mRNA-low initial conditions (Figure 6C-D, blue in center panels). Next, we varied the noise level in both systems, finding that the bimodal distributions were retained with the diverging oscillator but not the bistable switch in both noise-reduced and noise-amplified situations (compare rows in Figure 6C-D; Supplementary Videos S1 and S2). Furthermore, when we changed the initial conditions to mRNA-high states, we observed significant alteration of gene expression patterns with the bistable switch under medium and low noise conditions, while the diverging oscillator was insensitive to the changes of initial conditions under all tested cases (compare blue and red populations in Figure 6C-D).

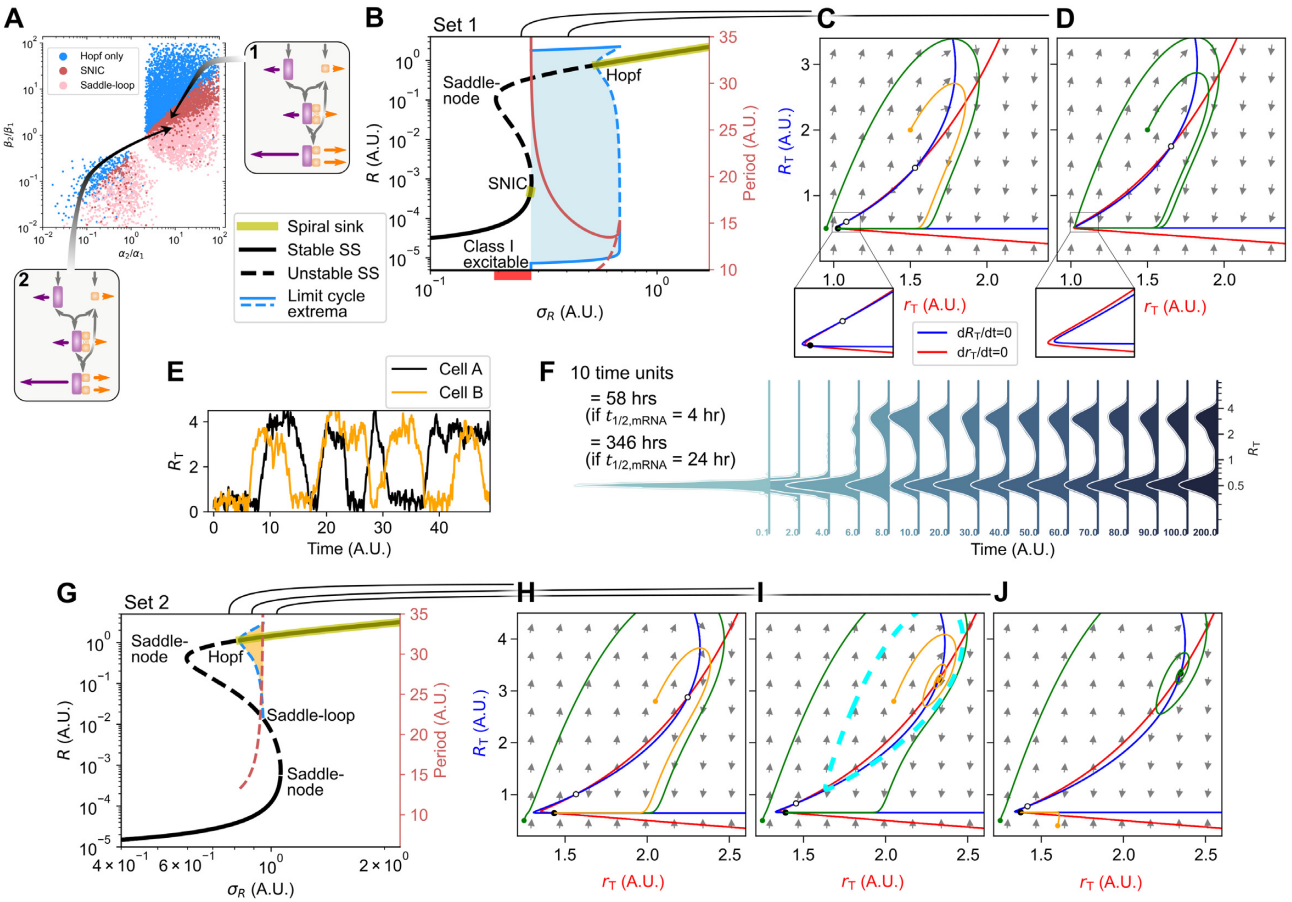

Figure 5. Global bifurcations of the MMI2-SSB Model. (**A**) Scatter plot shows parameter sets producing only Hopf bifurcation (blue) and those producing both Hopf and saddle-node bifurcations (same as Figure 3 dark blue) in the space of RDF ratios. Two representative sets are shown in callouts. (**B**) Bifurcation diagram shows levels of R in response to transcription rate constant σ_R. Blue shade: limit cycles' inner basins of attraction. (**C-D**) Phase planes show vector fields (gray), nullclines (red and blue), and representative solutions (green and orange) for $\sigma_R = 0.27$ and $\sigma_R = 0.4$, respectively. Open and closed circles represent unstable and stable steady states respectively. Other parameter values: $K = 0.001, \gamma = 0.25, \alpha_1 = \beta_1 = 1, \alpha_2 = 12, \beta_2 = 4$, and basal mRNA synthesis rate $\sigma_R^0 = 5.7$. (**E**) Trajectories of stochastic simulation for two representative cells under a SNIC parameter set. Stochastic ODEs have the form $dx = f(x)dt + \omega_x dW$, where x represents either R or r, $f(x)$ is the right-hand side of the first two ODEs in equation 2, and dW denotes the Wiener process. $\omega_R = 1.4$. $\omega_r = 0.35$. $\sigma_R = 0.3$. Other parameter values are the same as in B-D. One time unit is approximately $1.44 \times t_{1/2}$ where $t_{1/2}$ is the half-life of the mRNA. The initial condition is the deterministic steady state solution obtained with $\sigma_R = 0.1$. (**F**) Distributions of total mRNA concentrations in 500 simulated cells at the indicated time points. Initial conditions and parameter values are identical to E. (**G**) Bifurcation diagram of a model exhibiting a saddle-loop bifurcation showing levels of R in response to transcription rate constant σ_R. Parameter values are the same as for B except $\beta_2 = 3$ and $\sigma_R^0 = 6.9$. (**H-J**) Phase planes show vector fields, nullclines, and representative solutions of the saddle-loop model for $\sigma_R = 0.7$, $\sigma_R = 0.85$, and $\sigma_R = 1$, respectively.

The pronounced robustness of bimodality regeneration by the diverging oscillator compared to the bistable switch was in agreement with the consistent quasi-potential landscapes at different noise levels (Supplementary Figure S10A-B). Intuitively, changing noise levels (e.g. by altering the environment or cell volume) can significantly vary the heights of the middle barriers in both mechanisms, but the barrier lies in the main routes of state transitions only for the bistable switch (Figure 6A-B, Supplementary Figure S10A-B) (72). In addition, we observed that the diverging oscillator produced bimodality in a wide range of σ_R (compare columns in Figure 6C-D), even when the limit cycles were absent (Supplementary Figure S10C). This is because the vector field characteristic of the limit cycle has a significant influence on its adjacent parameter region. Furthermore, for systems that have only Hopf bifurcations (Figure 3B) and those have saddle-loop but not SNIC bifurcations (Figure 5G), the double-channel-double-well landscapes were still retained (Supplementary Figure S10D-E). These results suggest that while SNIC bifurcation occurs in a small parameter region, it acts as an organizing center for the diverging oscillator that can be supported by widely distributed parameter values (Figure 5A).

Next, we performed a more systematic comparison between three types of diverging oscillators (SNIC, saddle-loop, and diverging Hopf) and a bistable switch with additional stochastic simulations and a metric of bimodality based on Gaussian mixture models (Figure 6E-F, Supplementary Table S2, Section 2.1.9 in Supplementary Data). We found that the diverging oscillators not only regenerated expression patterns with nonlinear time courses of cell fractions observed experimentally (Figure 6E) (2), but also produced wider ranges of bimodality compared to the

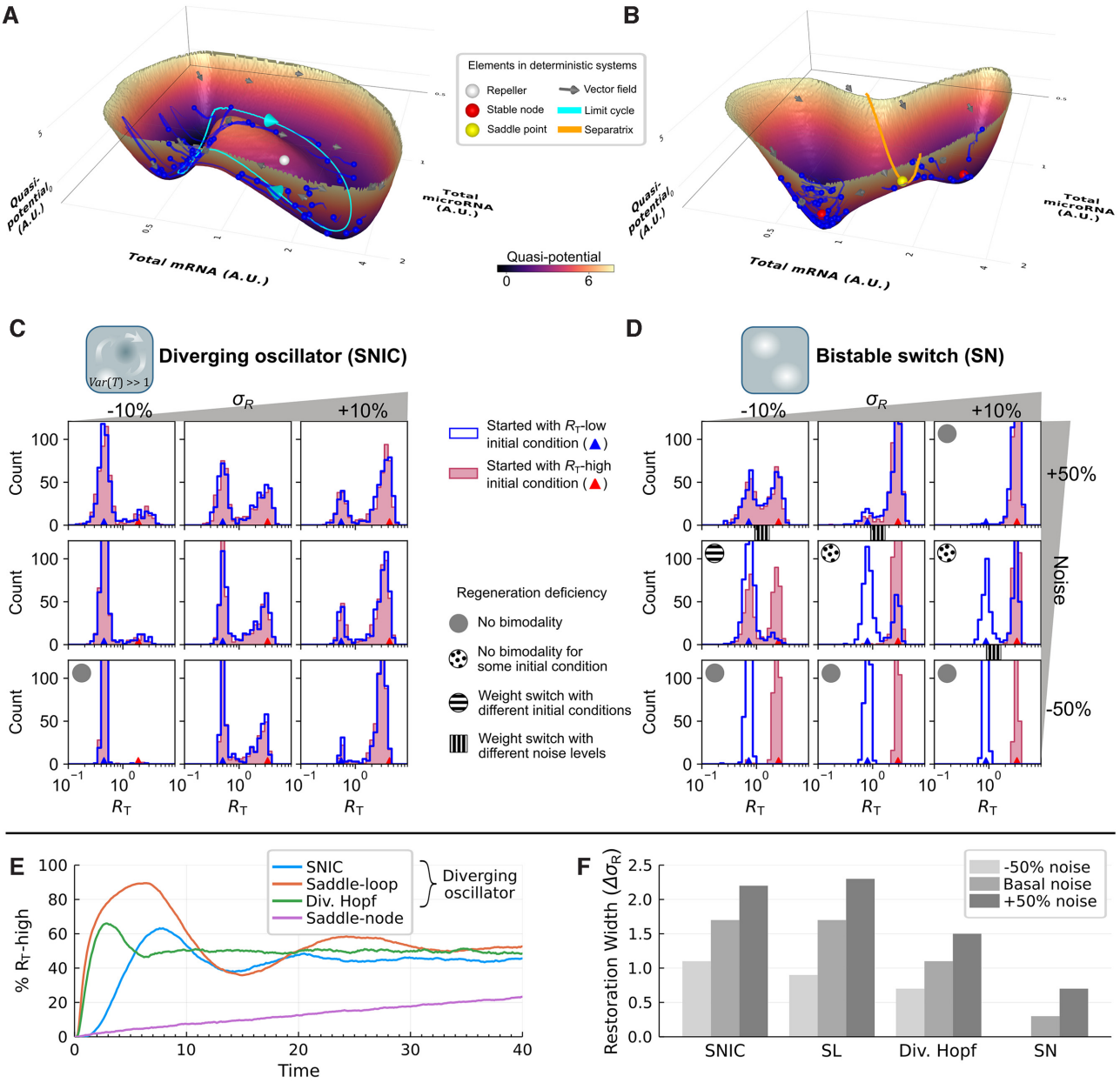

Figure 6. Comparison of MMI2-SSB mechanisms for regenerating bimodal gene expression distributions. (**A-B**) Landscapes of the MMI2-SSB Model with additive noise describing stochastic transcription of mRNA and microRNA (basal noise level ,). Landscapes were computed based on stationary phase distribution of stochastic simulations of 500 cells. For each landscape, 50 cells were randomly selected and visualized with the positions at $t = 50$ (blue spheres) and trajectories in a 0.4 time-unit period (blue tails). Parameter values for the model generating SNIC bifurcation (A) are the same as in Figure 5B. Parameter values for the model generating SN bifurcation (B) are as in Figure 3F. (**C-D**) Distributions of total mRNA concentrations at $t = 100$ (576 hours after selecting cells with extreme expression, assuming a 4-hour mRNA half-life) with three values of σ_R, three levels of noise, two initial conditions, and two switch mechanisms from A and B. Noise levels for both mechanisms were identical in corresponding panels. The basal noise levels (middle row) are as in A and B. The σ_R values for the two middle columns are 0.3 and 3.2 for the two mechanisms, respectively. The R_T-low and R_T-high initial conditions were obtained by sampling 400 initial conditions and their corresponding extrema in the period $t > 5$. (**E**) Early timecourse of the proportion of R_T-high cells in a 5000-cell population starting from the low initial condition under basal noise for several MMI2-SSB Models. For SNIC, with R_T cutoff 1.0; for the saddle-loop (SL) model in Figure 5G, with cutoff 1.25; for the diverging (div.) Hopf model in Figure 3B, with cutoff 0.75; for saddle-node, with cutoff 1.3. All other parameters are compiled in Supplementary Table S2. (**F**) Width of the region of σ_R in which each model in E can restore bimodal gene expression.

bistable switch (Figure 6F, Supplementary Figure S12, Supplementary Table S3). Since all the MMI2-driven oscillations are diverging, we performed the same analysis with two previously known non-diverging oscillators (Section 4 in Supplementary Data, Supplementary Tables S5 and S6), the repressilator (42) and a "genetic oscillator" (43), and confirmed that the non-diverging oscillators do not produce bimodality as robustly (Supplementary Figures S19 and S20). We used two alternative approaches, multiplicative noise and the Gillespie algorithm, to model noise in the MMI2-SSB Model, confirming that our conclusions about the capabilities of the diverging oscillator are not sensitive to the types of noise (Supplementary Figures S11, S13, and S14). Finally, we explicitly incorporated cell division into the model, confirming that the results are applicable to the scenario of a proliferating cell population during heterogeneity recovery (Figure 1 box, Supplementary Figure S15).

In conclusion, the diverging oscillator mechanism based on the MM2-SSB Model gave rise to more robust regeneration of multimodality gene expression patterns compared to the commonly used bistable switch mechanism. Nonetheless, our results do not imply that the diverging oscillator is the only mechanism for dynamics of all cells in a population of progenitor cells, which may contain both self-regenerative cells that exhibit reversible transitions and those stabilized in point attractors (10). Remarkably, the MMI2-SSB Model can support either mechanism with adjustment of rate constants.

Sustained oscillation and bistability are achieved without structural modularity

We have shown that the diverging oscillators arise from adjacent limit cycles and saddle-node bifurcation points, which further suggests that the emergent functions of the MMI2 Models depend on their capacity of producing both oscillations and bistable switches. Bifunctional systems are often evaluated to consider whether the two functions are governed by distinct subnetworks. We therefore asked whether a MMI2 Model contains two molecular modules each responsible for one function. According to the definition by Jiménez et al. (77), the degree of modularity regarding two biological functions generated by a network can be described by the number of molecular species (e.g. genes) shared by two subnetworks necessary for achieving the two functions respectively, divided by number of molecular species in the union of the two subnetworks. This quantity is the Jaccard index

$$J(A, B) = \frac{|A \cap B|}{|A \cup B|}, \quad (4)$$

where A and B are sets of nodes of the two subnetworks necessary to achieve the two functions respectively. If the two subnetworks overlap completely in terms of the structural components ($J = 1$), then the two functions are completely structurally nonmodular in this network. This scenario has a profound implication in evolution: the acquisition of a new function does not require the inclusion of any new molecular species to the existing network; instead, the function can be obtained simply by adjusting the kinetic rate constants in the existing network.

To what extent are bistability and oscillation structurally modular in the MMI2 Models? Addressing this question requires the identification of essential molecular species for bistability and oscillation respectively. We focused on two variants of the MMI2 Model that we described earlier: the MMI2-SSB Model where the two binding sites were assumed to be identical (the simplest biological assumption), and the MMI2-ASB Model where only a unique 1:1 complex is possible (a model structurally simpler than the MMI2-SSB Model). We first asked whether the 2:1 complex is required for bistability and oscillation. Removing the reaction responsible for the formation of the 2:1 complex from the MMI2-ASB Model gave rise to the structure of the MMI1 Model which always converges to a point attractor (Figures 2 and 7A, Row 1). Removing the same reaction from the MMI2-SSB Model gave rise to a similar model (the C2KO Model in Figure 7A, Row 2). We found that neither oscillation nor bistability can be obtained with the C2KO Model, i.e. none of the randomly generated 10^5 parameter sets produced Hopf bifurcation or saddle-node bifurcation. We proceeded to prove this analytically. We found that the C2KO Model has at most one positive steady state, which is asymptotically stable (Section 3.1 in Supplementary Data, Supplementary Figure S17). As a consequence, the C2KO Model is incapable of generating oscillations or bistability. The 2:1 complex is therefore required for both functions. To test whether a 1:1 complex is required for bistability and oscillation, we assumed that the second binding site is occupied immediately upon the binding of the first site in both MMI2-SSB and MMI2-ASB Models, which gave rise to the C1KO Model (Figure 7A, bottom right). With this modification, both oscillation and bistability were lost completely (Figure 7A, Row 3; see Section 3.2 and Supplementary Figure S18 in Supplementary Data for an analytical proof), suggesting that a 1:1 complex is also required to achieve both functions. Because the unbound forms of the mRNA and the miRNA are required to form the complexes, which cannot be produced through transcription directly, it is impossible to remove these unbound species in a biologically meaningful way without removing the complexes. Removing the transcription reaction of either unbound miRNA or unbound mRNA resulted in trivial cases in which the system has a single point attractor (Figure 7A, Rows 4 and 5). In addition, significant amounts of each of the unbound mRNA species always appeared in some phases of the sustained oscillations (Figure 3C). Similarly, in each bistable system observed with the MMI2-SSB and MMI2-ASB Models, unbound mRNA and unbound miRNA existed in at least one stable steady state. We therefore concluded that the unbound species are required for both bistability and oscillation. Taken together, we found that there is no structural modularity of bistability and oscillation in the MMI2 Model ($J = 1$, right endpoint of Figure 7B; Supplementary Table S4).

DISCUSSION

MicroRNA-mediated gene expression variation

MicroRNA has been extensively studied in its roles in attenuating noise and increasing phenotypic robustness (19). However, recent data suggest that some microRNA can

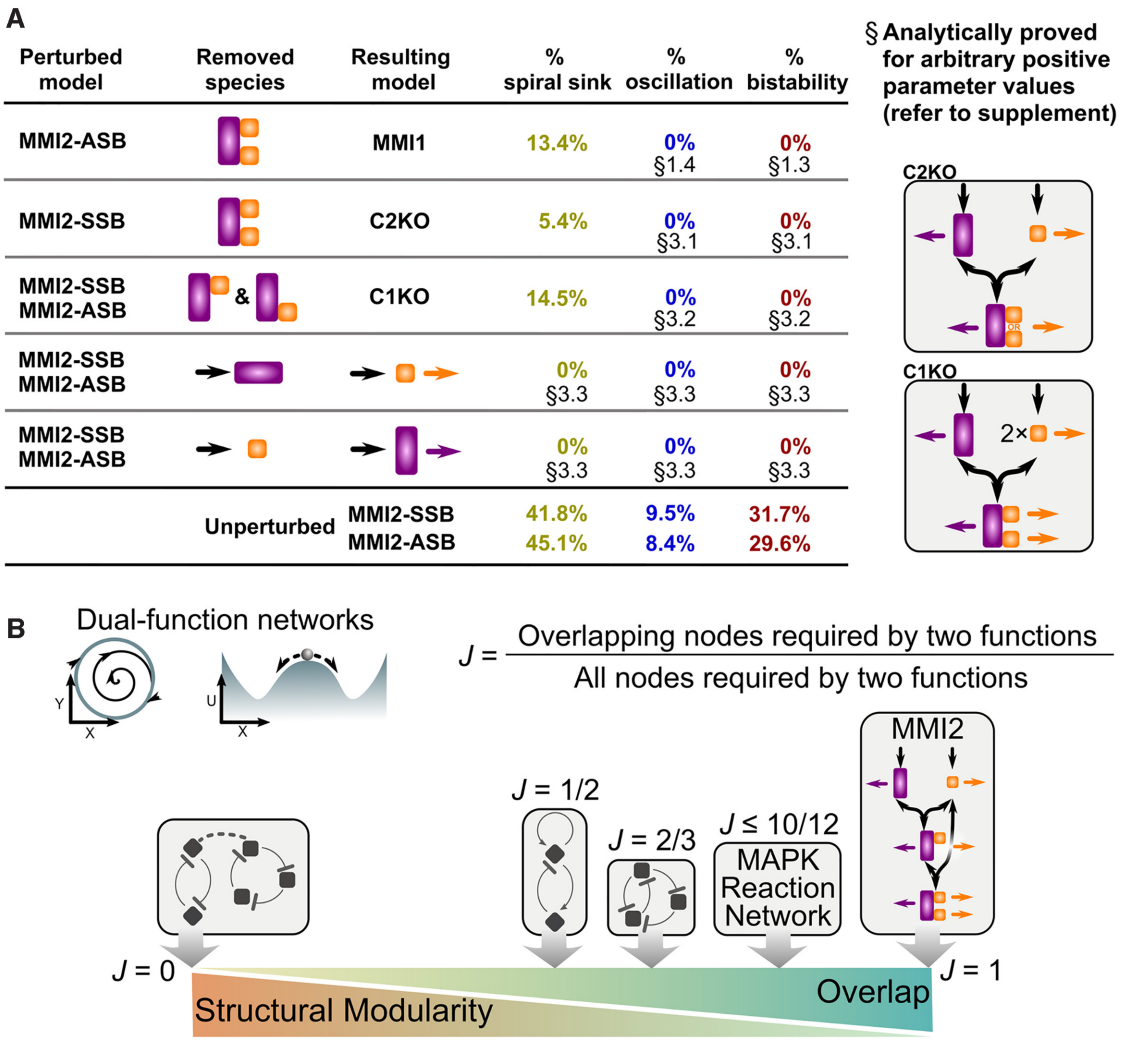

Perturbed model	Removed species	Resulting model	% spiral sink	% oscillation	% bistability
MMI2-ASB		MMI1	13.4%	0% §1.4	0% §1.3
MMI2-SSB		C2KO	5.4%	0% §3.1	0% §3.1
MMI2-SSB MMI2-ASB	&	C1KO	14.5%	0% §3.2	0% §3.2
MMI2-SSB MMI2-ASB			0% §3.3	0% §3.3	0% §3.3
MMI2-SSB MMI2-ASB			0% §3.3	0% §3.3	0% §3.3
	Unperturbed	MMI2-SSB MMI2-ASB	41.8% 45.1%	9.5% 8.4%	31.7% 29.6%

Figure 7. Nonmodular combination of two functions in the MMI2 Models. (**A**) Table shows five biologically plausible ways for removing molecular species from the MMI2-SSB or the MMI2-ASB Models. For each model, 10^5 parameter sets were randomly generated. Percentages of indicated steady state behaviors through bifurcation analysis with respect to σ_R are shown in the last three columns. In all cases, 0% means that exactly none of the 10^5 sets produced the indicated type of steady state. Bottom rows show the performance of the unperturbed MMI2-SSB and MMI2-ASB Models. Right diagrams show structures of the two new perturbed models. (B) Summary of the structural modularity (quantified by the Jaccard index) of representative networks containing sustained oscillation and bistability. The Jaccard indices of the combined toggle-switch-repressilator circuit and the MAPK network were estimated based on previous work (82,85).

increase gene expression fluctuations and facilitate phenotypic variation (8,20). Nonetheless, previous theories of miRNA dynamics assume that microRNA-mRNA interactions alone do not produce oscillatory or excitable systems (23,78). Our results raise the possibility that some microRNAs may induce slow-timescale oscillatory dynamics without a transcription-dependent feedback loop. This suggests that the observed variation-amplifying effects of miRNA may be due to limit cycle oscillations or excitability resulting from simple reaction networks of microRNA and mRNA. We showed that the oscillatory and excitable dynamics can be obtained with several versions of the MMI2 Model. Furthermore, our conclusions were not sensitive to the assumption that the two RNAs are only degraded separately rather than co-degraded (Supplementary Figure S21), suggesting the robustness of the emergent dynamics. These destabilizing dynamics at the post-transcriptional level may provide additional strategies for cells to encode and process information, or to regenerate heterogeneity in cell populations.

Modularity of oscillators and bistable switches

Negative and positive feedback loops have been considered essential components for biological rhythms and switches, respectively (17,79,80). Consistent with the difference in structure between the two feedback loops, each of the previously studied biological networks with both switch and rhythm functions contains two distinct modules, which may have partial, but not complete, overlap in terms of molecular species (e.g. gene products) (81–87). Here, we showed the possibility that the two functions may not have any structural modularity in the RNA-centric reaction networks,

which highlights the importance of functional modularity when studying biological networks (77,88). Furthermore, this work revealed broad ranges of kinetic rate constants allowing oscillation and bistability in the MMI2 Models, which may guide synthetic biologists to design RNA-based circuits with versatile functions.

Comparison with other dual oscillator-switches

It was previously shown that the MAPK cascade, a widely studied protein signaling network, produces both oscillation and bistability (89). The periods of the oscillations generated by the protein network (about 30 min) are much shorter than those generated by the MMI2 Models. It was recently found that some molecular species in the MAPK network are required for bistability, but not oscillation (85), indicating structural modularity in the network. Nonetheless, because of the highly integrated structural components, we expect that the MAPK network shares some of the emergent properties that we discussed for the RNA-based diverging oscillator (e.g. global bifurcations), and it will be important to investigate the mathematical basis of these oscillator-switches collectively in the future.

Another recent study combined a repressilator and toggle-switch to generate a dual-function circuit based on transcriptional regulations (82). To achieve both oscillation and bistability in similar parameter regions, the circuit requires an additional feed-forward loop at the signal level. Furthermore, the combined circuit is structurally modular with respect to the two functions (82). Finally, due to the long distance between the orbit and the point attractors in the state space, global bifurcations and subcritical Hopf bifurcation, which also contain global features (79,80), are relatively rare with the circuit (82). All these properties are distinct from those of the diverging oscillator studied here.

With a network containing nine transcriptional regulations, Jutras-Dubé et al. recently showed the superior robustness of SNIC bifurcation in generating embryonic patterns compared to Hopf bifurcation (90). The MMI2 Models provide a simple mechanism for generating such global bifurcation at the post-transcriptional level, which could be used for patterning in early development. While it may be possible for a system to achieve dual functions through paradoxical feedback involving one transcription factor (TF) that both activates and inhibits a target gene directly (9,91), the paradoxical regulation requires two TF-promoter complexes responsible for activation and inhibition respectively (92), which would suggest a fundamental structural modularity.

Robust regeneration of multimodal gene expression patterns

Spontaneous regeneration of cell populations with multimodal gene expression patterns was observed in progenitor cells and cancer cells, but the mechanism for this phenomenon at slow time scales has been a longstanding problem in biology. While noise-induced transitions between stable steady states (point attractors) have been used to explain some of the observations, it was shown that the modality of the gene expression distribution and its underlying "epigenetic landscape" is very sensitive to the level of noise (93). We showed that oscillations with diverging periods can be useful to regenerate multimodal gene expression. In this mechanism, transitions between very distinct cell states are supported by both deterministic and stochastic dynamics: limit cycles and excitable vector fields ensure the periodic occurrence of dramatic change of gene expression, whereas stochasticity is important for producing the asynchrony in the cell population, and for triggering the oscillatory responses in some cases. The possibility of using excitable systems to generate multimodal expression pattern was discussed previously (9).

As this study examined the dynamics of generalized models, it cannot identify specific networks involved in observed heterogeneity restoration processes. Determining how many real mRNA-microRNA networks fall into the parameter regions responsible for these dynamics would require detailed experimental measurements. The models furthermore do not incorporate impacts on RNA decay or noise levels by other dynamic cellular processes, which may enhance or suppress variation in expression.

Nevertheless, our work showed a simple and potentially widespread mechanism to achieve period-diverging oscillations. This hitherto unknown mechanism can help researchers discover circuits responsible for regenerating heterogenous populations of specific cell types.

DATA AVAILABILITY

Computer code for reproducing results in this study is available at https://github.com/lfsc507/MMI2. This study did not produce any experimental data.

SUPPLEMENTARY DATA

Supplementary Data are available at NAR Online.

ACKNOWLEDGEMENTS

The authors thank Chunhe Li and John Tyson for helpful discussions.
Author contributions: Conceptualization: TH. Formal analysis: PYY and TH. Funding acquisition: TH. Investigation: BN, PYY, GL, and TH. Software: BN and TH. Visualization: BN and TH. Writing: BN, PYY, and TH. All the authors read and approved the manuscript.

FUNDING

National Institutes of Health [R01GM140462 to T.H.]. Funding for open access charge: National Institutes of Health.
Conflict of interest statement. None declared.

REFERENCES

1. Jordan,N.V., Bardia,A., Wittner,B.S., Benes,C., Ligorio,M., Zheng,Y., Yu,M., Sundaresan,T.K., Licausi,J.A. and Desai,R. (2016) HER2 expression identifies dynamic functional states within circulating breast cancer cells. *Nature*, **537**, 102–106.
2. Chang,H.H., Hemberg,M., Barahona,M., Ingber,D.E. and Huang,S. (2008) Transcriptome-wide noise controls lineage choice in mammalian progenitor cells. *Nature*, **453**, 544–547.

3. Shaffer,S.M., Dunagin,M.C., Torborg,S.R., Torre,E.A., Emert,B., Krepler,C., Beqiri,M., Sproesser,K., Brafford,P.A. and Xiao,M. (2017) Rare cell variability and drug-induced reprogramming as a mode of cancer drug resistance. *Nature*, **546**, 431.
4. Spencer,S.L., Gaudet,S., Albeck,J.G., Burke,J.M. and Sorger,P.K. (2009) Non-genetic origins of cell-to-cell variability in TRAIL-induced apoptosis. *Nature*, **459**, 428–432.
5. Min,M. and Spencer,S.L. (2019) Spontaneously slow-cycling subpopulations of human cells originate from activation of stress-response pathways. *PLoS Biol.*, **17**, e3000178.
6. Peláez,N., Gavalda-Miralles,A., Wang,B., Navarro,H.T., Gudjonson,H., Rebay,I., Dinner,A.R., Katsaggelos,A.K., Amaral,L.A.N. and Carthew,R.W. (2015) Dynamics and heterogeneity of a fate determinant during transition towards cell differentiation. *Elife*, **4**, e08924.
7. Abranches,E., Guedes,A.M.V., Moravec,M., Maamar,H., Svoboda,P., Raj,A. and Henrique,D. (2014) Stochastic NANOG fluctuations allow mouse embryonic stem cells to explore pluripotency. *Development*, **141**, 2770–2779.
8. Chakraborty,M., Hu,S., Visness,E., Del Giudice,M., De Martino,A., Bosia,C., Sharp,P.A. and Garg,S. (2020) MicroRNAs organize intrinsic variation into stem cell states. *Proc. Natl. Acad. Sci. USA*, **117**, 6942–6950.
9. Kalmar,T., Lim,C., Hayward,P., Muñoz-Descalzo,S., Nichols,J., Garcia-Ojalvo,J. and Martinez Arias,A. (2009) Regulated fluctuations in nanog expression mediate cell fate decisions in embryonic stem cells. *PLoS Biol.*, **7**, e1000149.
10. Pina,C., Fugazza,C., Tipping,A.J., Brown,J., Soneji,S., Teles,J., Peterson,C. and Enver,T. (2012) Inferring rules of lineage commitment in haematopoiesis. *Nat. Cell Biol.*, **14**, 287–294.
11. Raj,A., Peskin,C.S., Tranchina,D., Vargas,D.Y. and Tyagi,S. (2006) Stochastic mRNA synthesis in mammalian cells. *PLoS Biol.*, **4**, e309.
12. Corrigan,A.M., Tunnacliffe,E., Cannon,D. and Chubb,J.R. (2016) A continuum model of transcriptional bursting. *Elife*, **5**, e13051.
13. Raj,A. and Van Oudenaarden,A. (2008) Nature, nurture, or chance: stochastic gene expression and its consequences. *Cell*, **135**, 216–226.
14. Huang,S. (2009) Non-genetic heterogeneity of cells in development: more than just noise. *Development*, **136**, 3853–3862.
15. Udomlumleart,T., Hu,S. and Garg,S. (2021) Lineages of embryonic stem cells show non-Markovian state transitions. *Iscience*, **24**, 102879.
16. Enver,T., Pera,M., Peterson,C. and Andrews,P.W. (2009) Stem cell states, fates, and the rules of attraction. *Cell Stem Cell*, **4**, 387–397.
17. Thomas,R. (1981) In: *Numerical methods in the study of critical phenomena*. Springer, pp. 180–193.
18. Miranda,K.C., Huynh,T., Tay,Y., Ang,Y.-S., Tam,W.-L., Thomson,A.M., Lim,B. and Rigoutsos,I. (2006) A pattern-based method for the identification of MicroRNA binding sites and their corresponding heteroduplexes. *Cell*, **126**, 1203–1217.
19. Li,X., Cassidy,J.J., Reinke,C.A., Fischboeck,S. and Carthew,R.W. (2009) A microRNA imparts robustness against environmental fluctuation during development. *Cell*, **137**, 273–282.
20. Schmiedel,J.M., Klemm,S.L., Zheng,Y., Sahay,A., Blüthgen,N., Marks,D.S. and van Oudenaarden,A. (2015) MicroRNA control of protein expression noise. *Science*, **348**, 128–132.
21. Wei,L., Li,S., Zhang,P., Hu,T., Zhang,M.Q., Xie,Z. and Wang,X. (2021) Characterizing microRNA-mediated modulation of gene expression noise and its effect on synthetic gene circuits. *Cell Reports*, **36**, 109573.
22. Bonev,B., Stanley,P. and Papalopulu,N. (2012) MicroRNA-9 modulates Hes1 ultradian oscillations by forming a double-negative feedback loop. *Cell Reports*, **2**, 10–18.
23. Li,C.J., Liau,E.S., Lee,Y.H., Huang,Y.Z., Liu,Z., Willems,A., Garside,V., McGlinn,E., Chen,J.A. and Hong,T. (2021) MicroRNA governs bistable cell differentiation and lineage segregation via a noncanonical feedback. *Mol. Syst. Biol.*, **17**, e9945.
24. Tian,X.J., Zhang,H., Zhang,J. and Xing,J. (2016) Reciprocal regulation between mRNA and microRNA enables a bistable switch that directs cell fate decisions. *FEBS Lett.*, **590**, 3443–3455.
25. Kim,J.K. and Tyson,J.J. (2020) Misuse of the Michaelis–Menten rate law for protein interaction networks and its remedy. *PLoS Comput. Biol.*, **16**, e1008258.
26. Borghans,J.A.M., De Boer,R.J. and Segel,L.A. (1996) Extending the quasi-steady state approximation by changing variables. *Bull. Math. Biol.*, **58**, 43–63.
27. Ciliberto,A., Capuani,F. and Tyson,J.J. (2007) Modeling networks of coupled enzymatic reactions using the total quasi-steady state approximation. *PLoS Comput. Biol.*, **3**, e45.
28. Choi,K., Medley,J.K., König,M., Stocking,K., Smith,L., Gu,S. and Sauro,H.M. (2018) Tellurium: An extensible python-based modeling environment for systems and synthetic biology. *Biosystems*, **171**, 74–79.
29. Clewley,R. (2012) Hybrid Models and Biological Model Reduction with PyDSTool. *PLoS Comput. Biol.*, **8**, e1002628.
30. Feinberg,M. (2019) In: *Foundations of Chemical Reaction Network Theory*. Springer International Publishing.
31. Routh,E.J. (1877) In: *A Treatise on the Stability of a Given State of Motion, Particularly Steady Motion: Being the Essay to which the Adams Prize was Adjudged in 1877, in the University of Cambridge*. Macmillan and Company.
32. Hurwitz,A. (1895) Ueber die Bedingungen, unter welchen eine Gleichung nur Wurzeln mit negativen reellen Theilen besitzt. *Mathematische Annalen*, **46**, 273–284.
33. Agarwal,V., Bell,G.W., Nam,J.-W. and Bartel,D.P. (2015) Predicting effective microRNA target sites in mammalian mRNAs. *eLife*, **4**, e05005.
34. Huang,H.-Y., Lin,Y.-C.-D., Li,J., Huang,K.-Y., Shrestha,S., Hong,H.-C., Tang,Y., Chen,Y.-G., Jin,C.-N. and Yu,Y. (2020) miRTarBase 2020: updates to the experimentally validated microRNA–target interaction database. *Nucleic Acids Res.*, **48**, D148–D154.
35. Tay,Y., Zhang,J., Thomson,A.M., Lim,B. and Rigoutsos,I. (2008) MicroRNAs to Nanog, Oct4 and Sox2 coding regions modulate embryonic stem cell differentiation. *Nature*, **455**, 1124–1128.
36. Nordick,B. and Hong,T. (2021) Identification, visualization, statistical analysis and mathematical modeling of high-feedback loops in gene regulatory networks. *BMC Bioinformatics*, **22**, 481.
37. Han,H., Cho,J.-W., Lee,S., Yun,A., Kim,H., Bae,D., Yang,S., Kim,C.Y., Lee,M., Kim,E. *et al.* (2018) TRRUST v2: an expanded reference database of human and mouse transcriptional regulatory interactions. *Nucleic Acids Res.*, **46**, D380–D386.
38. Rackauckas,C. and Nie,Q. (2017) Differentialequations. jl–a performant and feature-rich ecosystem for solving differential equations in julia. *J. Open Res. Software*, **5**, 15.
39. Li,C. and Wang,J. (2014) Landscape and flux reveal a new global view and physical quantification of mammalian cell cycle. *Proc. Natl. Acad. Sci. USA*, **111**, 14130–14135.
40. Thomas,P., Straube,A.V. and Grima,R. (2012) The slow-scale linear noise approximation: an accurate, reduced stochastic description of biochemical networks under timescale separation conditions. *BMC Syst. Biol.*, **6**, 39.
41. Kim,J.K., Josić,K. and Bennett,M.R. (2015) The relationship between stochastic and deterministic quasi-steady state approximations. *BMC Syst. Biol.*, **9**, 87.
42. Elowitz,M.B. and Leibler,S. (2000) A synthetic oscillatory network of transcriptional regulators. *Nature*, **403**, 335–338.
43. Kim,J.K., Josić,K. and Bennett,M.R. (2014) The validity of quasi-steady-state approximations in discrete stochastic simulations. *Biophys J.*, **107**, 783–793.
44. Song,Y.M., Hong,H. and Kim,J.K. (2021) Universally valid reduction of multiscale stochastic biochemical systems using simple non-elementary propensities. *PLoS Comput. Biol.*, **17**, e1008952.
45. Muratov,A.L. and Gnedin,O.Y. (2010) Modeling the metallicity distribution of globular clusters. *Astrophys. J.*, **718**, 1266–1288.
46. Eichhorn,S.W., Guo,H., McGeary,S.E., Rodriguez-Mias,R.A., Shin,C., Baek,D., Hsu,S.-h., Ghoshal,K., Villén,J. and Bartel,D.P. (2014) mRNA destabilization is the dominant effect of mammalian microRNAs by the time substantial repression ensues. *Mol. Cell*, **56**, 104–115.
47. de la Mata,M., Gaidatzis,D., Vitanescu,M., Stadler,M.B., Wentzel,C., Scheiffele,P., Filipowicz,W. and Großhans,H. (2015) Potent degradation of neuronal miRNAs induced by highly complementary targets. *EMBO Rep.*, **16**, 500–511.
48. Baccarini,A., Chauhan,H., Gardner,T.J., Jayaprakash,A.D., Sachidanandam,R. and Brown,B.D. (2011) Kinetic analysis reveals the fate of a microRNA following target regulation in mammalian cells. *Curr. Biol.*, **21**, 369–376.
49. Ghini,F., Rubolino,C., Climent,M., Simeone,I., Marzi,M.J. and Nicassio,F. (2018) Endogenous transcripts control miRNA levels and

activity in mammalian cells by target-directed miRNA degradation. *Nat. Commun.*, **9**, 3119.
50. Strogatz,S.H. (2018) In: *Nonlinear Dynamics and Chaos: With Applications to Physics, Biology, Chemistry and Engineering*. CRC press.
51. Mukherji,S., Ebert,M.S., Zheng,G.X.Y., Tsang,J.S., Sharp,P.A. and van Oudenaarden,A. (2011) MicroRNAs can generate thresholds in target gene expression. *Nat. Genet.*, **43**, 854.
52. Sharova,L.V., Sharov,A.A., Nedorezov,T., Piao,Y., Shaik,N. and Ko,M.S.H. (2009) Database for mRNA half-life of 19 977 genes obtained by DNA microarray analysis of pluripotent and differentiating mouse embryonic stem cells. *DNA Res.*, **16**, 45–58.
53. Grimson,A., Farh,K.K.-H., Johnston,W.K., Garrett-Engele,P., Lim,L.P. and Bartel,D.P. (2007) MicroRNA targeting specificity in mammals: determinants beyond seed pairing. *Mol. Cell*, **27**, 91–105.
54. Zlotorynski,E. (2019) Insights into the kinetics of microRNA biogenesis and turnover. *Nat. Rev. Mol. Cell Biol.*, **20**, 511–511.
55. McGlinn,E., Yekta,S., Mansfield,J.H., Soutschek,J., Bartel,D.P. and Tabin,C.J. (2009) In ovo application of antagomiRs indicates a role for miR-196 in patterning the chick axial skeleton through Hox gene regulation. *Proc. Natl. Acad. Sci. USA*, **106**, 18610–18615.
56. Novák,B. and Tyson,J.J. (2008) Design principles of biochemical oscillators. *Nat. Rev. Mol. Cell Biol.*, **9**, 981–991.
57. Ha,S.H. and Ferrell Jr,J.E. (2016) Thresholds and ultrasensitivity from negative cooperativity. *Science*, **352**, 990–993.
58. Cursons,J., Pillman,K.A., Scheer,K.G., Gregory,P.A., Foroutan,M., Hediyeh-Zadeh,S., Toubia,J., Crampin,E.J., Goodall,G.J., Bracken,C.P. *et al.* (2018) Combinatorial Targeting by MicroRNAs Co-ordinates Post-transcriptional Control of EMT. *Cell Systems*, **7**, 77–91.
59. Buck,A.H., Coakley,G., Simbari,F., McSorley,H.J., Quintana,J.F., Le Bihan,T., Kumar,S., Abreu-Goodger,C., Lear,M. and Harcus,Y. (2014) Exosomes secreted by nematode parasites transfer small RNAs to mammalian cells and modulate innate immunity. *Nat. Commun.*, **5**, 5488.
60. Lai,X., Eberhardt,M., Schmitz,U. and Vera,J. (2019) Systems biology-based investigation of cooperating microRNAs as monotherapy or adjuvant therapy in cancer. *Nucleic Acids Res.*, **47**, 7753–7766.
61. Phillips,N.E., Manning,C.S., Pettini,T., Biga,V., Marinopoulou,E., Stanley,P., Boyd,J., Bagnall,J., Paszek,P. and Spiller,D.G. (2016) Stochasticity in the miR-9/Hes1 oscillatory network can account for clonal heterogeneity in the timing of differentiation. *eLife*, **5**, e16118.
62. Zhou,Z., Shu,B., Xu,Y., Liu,J., Wang,P., Chen,L., Zhao,J., Liu,X., Qi,S. and Xiong,K. (2018) microRNA-203 modulates wound healing and scar formation via suppressing Hes1 expression in epidermal stem cells. *Cell. Physiol. Biochem.*, **49**, 2333–2347.
63. Gao,Q., Zhou,L., Yang,S.-Y. and Cao,J.-M. (2016) A novel role of microRNA 17-5p in the modulation of circadian rhythm. *Sci. Rep.*, **6**, 30070.
64. Wang,F., Zhu,Y., Guo,L., Dong,L., Liu,H., Yin,H., Zhang,Z., Li,Y., Liu,C. and Ma,Y. (2014) A regulatory circuit comprising GATA1/2 switch and microRNA-27a/24 promotes erythropoiesis. *Nucleic Acids Res.*, **42**, 442–457.
65. Li,C.-J., Hong,T., Tung,Y.-T., Yen,Y.-P., Hsu,H.-C., Lu,Y.-L., Chang,M., Nie,Q. and Chen,J.-A. (2017) MicroRNA filters Hox temporal transcription noise to confer boundary formation in the spinal cord. *Nat. Commun.*, **8**, 14685.
66. Burk,U., Schubert,J., Wellner,U., Schmalhofer,O., Vincan,E., Spaderna,S. and Brabletz,T. (2008) A reciprocal repression between ZEB1 and members of the miR-200 family promotes EMT and invasion in cancer cells. *EMBO Rep.*, **9**, 582–589.
67. Pan,W., Zhu,S., Dai,D., Liu,Z., Li,D., Li,B., Gagliani,N., Zheng,Y., Tang,Y. and Weirauch,M.T. (2015) MiR-125a targets effector programs to stabilize Treg-mediated immune homeostasis. *Nat. Commun.*, **6**, 7096.
68. Ma,F., Xu,S., Liu,X., Zhang,Q., Xu,X., Liu,M., Hua,M., Li,N., Yao,H. and Cao,X. (2011) The microRNA miR-29 controls innate and adaptive immune responses to intracellular bacterial infection by targeting interferon-γ. *Nat. Immunol.*, **12**, 861–869.
69. Walker,S.E., Sabin,K.Z., Gearhart,M.D., Yamamoto,K. and Echeverri,K. (2022) Regulation of stem cell identity by miR-200a during spinal cord regeneration. *Development*, **149**, dev200033.
70. Sætrom,P., Heale,B.S.E., Snøve Jr,O., Aagaard,L., Alluin,J. and Rossi,J.J. (2007) Distance constraints between microRNA target sites dictate efficacy and cooperativity. *Nucleic Acids Res.*, **35**, 2333–2342.
71. Ermentrout,B. (1996) Type I membranes, phase resetting curves, and synchrony. *Neural Comput.*, **8**, 979–1001.
72. Li,C. and Wang,J. (2013) Quantifying cell fate decisions for differentiation and reprogramming of a human stem cell network: landscape and biological paths. *PLoS Comput. Biol.*, **9**, e1003165.
73. Moris,N., Pina,C. and Arias,A.M. (2016) Transition states and cell fate decisions in epigenetic landscapes. *Nat. Rev. Genet.*, **17**, 693–703.
74. Tian,X.-J., Zhang,H. and Xing,J. (2013) Coupled reversible and irreversible bistable switches underlying TGFβ-induced epithelial to mesenchymal transition. *Biophys. J.*, **105**, 1079–1089.
75. Hong,T., Watanabe,K., Ta,C.H., Villarreal-Ponce,A., Nie,Q. and Dai,X. (2015) An Ovol2-Zeb1 mutual inhibitory circuit governs bidirectional and Multi-step transition between epithelial and mesenchymal states. *PLoS Comput. Biol.*, **11**, e1004569.
76. Ye,Y., Kang,X., Bailey,J., Li,C. and Hong,T. (2019) An enriched network motif family regulates multistep cell fate transitions with restricted reversibility. *PLoS Comput. Biol.*, **15**, e1006855.
77. Jiménez,A., Cotterell,J., Munteanu,A. and Sharpe,J. (2017) A spectrum of modularity in multi-functional gene circuits. *Mol. Syst. Biol.*, **13**, 925.
78. Osella,M., Bosia,C., Corá,D. and Caselle,M. (2011) The role of incoherent microRNA-mediated feedforward loops in noise buffering. *PLoS Comput. Biol.*, **7**, e1001101.
79. Tyson,J.J., Chen,K.C. and Novak,B. (2003) Sniffers, buzzers, toggles and blinkers: dynamics of regulatory and signaling pathways in the cell. *Curr. Opin. Cell Biol.*, **15**, 221–231.
80. Tian,X.-J., Zhang,X.-P., Liu,F. and Wang,W. (2009) Interlinking positive and negative feedback loops creates a tunable motif in gene regulatory networks. *Physical Review E*, **80**, 011926.
81. Gelens,L., Anderson,G.A. and Ferrell Jr,J.E. (2014) Spatial trigger waves: positive feedback gets you a long way. *Mol. Biol. Cell*, **25**, 3486–3493.
82. Perez-Carrasco,R., Barnes,C.P., Schaerli,Y., Isalan,M., Briscoe,J. and Page,K.M. (2018) Combining a toggle switch and a repressilator within the AC-DC circuit generates distinct dynamical behaviors. *Cell Systems*, **6**, 521–530.
83. Iglesias,P.A. and Devreotes,P.N. (2012) Biased excitable networks: how cells direct motion in response to gradients. *Curr. Opin. Cell Biol.*, **24**, 245–253.
84. Rubinstein,B.Y., Mattingly,H.H., Berezhkovskii,A.M. and Shvartsman,S.Y. (2016) Long-term dynamics of multisite phosphorylation. *Mol. Biol. Cell*, **27**, 2331–2340.
85. Obatake,N., Shiu,A., Tang,X. and Torres,A. (2019) Oscillations and bistability in a model of ERK regulation. *J. Math. Biol.*, **79**, 1515–1549.
86. Moenke,G., Cristiano,E., Finzel,A., Friedrich,D., Herzel,H., Falcke,M. and Loewer,A. (2017) Excitability in the p53 network mediates robust signaling with tunable activation thresholds in single cells. *Sci. Rep.*, **7**, 46571.
87. Liu,Y., Rens,E.G. and Edelstein-Keshet,L. (2021) Spots, stripes, and spiral waves in models for static and motile cells. *J. Math. Biol.*, **82**, 28.
88. Verd,B., Monk,N.A.M. and Jaeger,J. (2019) Modularity, criticality, and evolvability of a developmental gene regulatory network. *Elife*, **8**, e42832.
89. Qiao,L., Nachbar,R.B., Kevrekidis,I.G. and Shvartsman,S.Y. (2007) Bistability and oscillations in the Huang-Ferrell model of MAPK signaling. *PLoS Comput. Biol.*, **3**, e184.
90. Jutras-Dubé,L., El-Sherif,E. and François,P. (2020) Geometric models for robust encoding of dynamical information into embryonic patterns. *Elife*, **9**, e55778.
91. Liu,Z., Shpak,E.D. and Hong,T. (2020) A mathematical model for understanding synergistic regulations and paradoxical feedbacks in the shoot apical meristem. *Comput. Struct. Biotechnol. J.*, **18**, 3877–3889.
92. Perales,M., Rodriguez,K., Snipes,S., Yadav,R.K., Diaz-Mendoza,M. and Reddy,G.V. (2016) Threshold-dependent transcriptional discrimination underlies stem cell homeostasis. *Proc. Natl. Acad. Sci. USA*, **113**, E6298–E6306.
93. Coomer,M.A., Ham,L. and Stumpf,M.P.H. (2021) Noise distorts the epigenetic landscape and shapes cell-fate decisions. *Cell Syst.*, **13**, 83–102.